THESIS

SPATIAL PRECIPITATION TRENDS AND EFFECTS OF CLIMATE CHANGE ON THE HAWAI'IAN HUALALAI AQUIFER

Submitted by

Alyssa Danielle Hendricks

Department of Ecosystem Science and Sustainability

In partial fulfillment of the requirements

For the Degree of Master of Science

Colorado State University

Fort Collins, Colorado

Spring 2015

Master's Committee:

Advisor: Steven Fassnacht

Melinda Laituri
Mazdak Arabi

ABSTRACT

SPATIAL PRECIPITATION TRENDS AND EFFECTS OF CLIMATE CHANGE ON THE HAWAI'IAN HUALALAI AQUIFER

While trends in temperature are well studied and understood spatially and temporally at a multitude of scales, trends in precipitation are less understood. As the predominant source of groundwater recharge in Western Hawai'i, precipitation plays a vital role in maintaining tourism and industry throughout the Kona Region. Kaloko-Honokohau National Historical Park was established in 1978 to perpetuate and maintain traditional native Hawai'ian culture and the surrounding ecosystem, which is dependent on freshwater from the surrounding Hualalai Aquifer. Precipitation increases with elevation from the coast to approximately 1500 meters up the slope of Hualalai Volcano and then decreases to approximately 2000 meters. Western Hawai'i has a dense rain gauge network and changes in precipitation in the last several decades have been observed, though the rate sand significance of change is unclear.

This study introduces a new method of integrated spatial analysis aimed at representing spatial trends in more detail. Using the Rainfall Atlas of Hawai'i, produced by the University of Hawai'i at Manoa, spatial trends from 1978-2007 were studied by annually adjusting the 30-year climate normal and calculating residuals between adjusted and observed precipitation. The Mann-Kendall and Sen's Slope statistical tests were used spatially to determine the rate and significance of change. This method was then compared with spatial interpolation by inverse distance weighting (IDW) and ordinary kriging to assess the differences in methods. Results from the integrated spatial analysis show an annual decrease of -8.42×10^6 m^3/year across the entire study area and a decrease of -4.62×10^6 m^3/year when only significant areas are considered. This can be

compared with -10.8 x 10^6 m^3/year total and -0.64 x 10^6 m^3/year in significant areas from IDW and -8.41 x 10^6 m^3/year and -1.31 x 10^6 m^3/year respectively from ordinary kriging. On a monthly basis, both the integrated spatial analysis and IDW yield similar trends regarding an increase or decrease in the net volume entering the aquifer, however IDW underestimates the overall magnitude. The introduced integrated spatial analysis method provides an improved assessment of spatial trends that, while not limited to precipitation, can assist in broadening the limited knowledge of spatial precipitation trends across the globe.

ACKNOWLEDGMENTS

This work would not have been possible without funding by the National Park Service award H2370094000 P10AC00658 entitled "Understanding the Historical & Potential Future Effects of Climate Change on Water-Dependent Cultural & Natural Resources. Also thanks to Colorado State University and the Warner College of Natural Resources for financial support allowing me to focus on classes and research. Thank you to my committee members, Melinda Laituri and Mazdak Arabi, for their insight and helpful reviews; Michael Koontz and Niah Venable for answering countless questions during the arduous process of learning R. Most importantly, thank you to my academic advisor, Steven Fassnacht, for not only help in development of my research project but also mentoring me through all aspects of graduate schoo

TABLE OF CONTENTS

1. INTRODUCTION

Changes in temperature have been extensively studied and are well understood across a wide range of temporal and spatial scales. The Fifth Assessment Report from the Intergovernmental Panel on Climate Change Working Group I illustrated that the globally averaged land surface air temperature has risen since the 19th century by an average increase of 0.72 degrees Celsius from 1951 to 2012, with the greatest amount of warming occurring since the 1970's (IPCC, 2013). However, trends in precipitation, globally and regionally, are less obvious. Precipitation in the tropics (30 degrees N to 30 degrees S latitude) has both decreased and increased since the 1970's; precipitation has increased in the last decade (2000's), reversing the drying trend observed from the 1970's to late 1990's (IPCC, 2013).

At smaller spatial scales minimum temperatures on the island of Oahu in Hawai'i, USA have an average increase of 0.17 degrees Celsius per decade (Safeeq et al., 2013) and the statewide average warming for Hawai'i is 0.2 degrees Celsius per decade since 1975 (Giambelluca et al., 2008). The complexity of precipitation trends is even greater when comparing changes at smaller spatial scales, as significant differences in annual precipitation trends have been observed across three islands in the Hawaiian Archipelago (Chen and Chu, 2014). The island of Hawai`i itself has seen a predominately positive annual precipitation trend, as well as precipitation intensity, though most of the increase is located in the high elevations surrounding Mt. Mauna Loa. Opposite trends, with decreasing precipitation intensity are seen on the much drier, western side of the island (Chu et al., 2010).

These localized and regional spatial patterns of precipitation dictate water resources on the island scale, with regions of highest precipitation home the highest resource availability (Hawai'i

County Water Use and Development Plan, 2010). Therefore, patterns then play a large role in resource management, especially in tropical island settings where freshwater resources quickly meet the ocean (Falkland, 1999). Changes in precipitation patterns lead to concerns for water resource management as extreme events, such as droughts and floods, will likely occur more frequently and with a higher severity in the future (Brekke et al., 2009). In Hawai`i in particular, declines in baseflow and low-streamflow have been noted across the entire Hawaiian Archipelago (Bassiouini and Oki, 2013); though only surface water records were used, the decline in flow indicate a long-term decrease in water resources availability statewide, including Kona where only minimal surface water is available (Hawai'i County Plan, 2010).

The variability in trends at differing spatial scales is shown by Pielke et al. (2002), who specifically noted that "highly localized unknown causes" of temperature variations could override regional and global forcings. Large-scale forcings that influence the climate of Hawai'i include the El Niño Southern Oscillation (ENSO) and Pacific Decadal Oscillation (PDO) (Chu and Chen, 2005). However, the differences in local and regional trends are important to consider when conducting any type of climatic study as conditions averaged over a large area may act to mask local anomalies, in both the magnitude and direction of climate change (Pielke et al., 2002). Since the island of Hawai`i has two very different climatic regimes depending on the side of the island (Figure 1), it is important to differentiate trends between the dry Kona and wet Hilo sides as an average trend over the entire island would likely result in underestimated precipitation in Hilo and overestimated precipitation in Kona.

Despite the lack of precipitation and surface water compared to the Hilo side of Hawai`i, Kona is highly dependent on available water resources, as the agriculture and tourism industries dominate water use in the region (Hawai'i County Plan, 2010). Kaloko-Honokohau National

Historical Park (KAHO) was established in 1978, aimed at conservation and perpetuation of traditional native activities, which are also dependent on the limited water resources on this side of the island. The purpose of this study is to present methodology for spatial trend analysis of both rate and significance of change, compare this method with point trend analysis, and use both to compute the net volume of change in precipitation falling over an aquifer system. This will be done in the context of better understanding spatial precipitation trends in Western Hawai'i for water resource implications related to KAHO and the surrounding area.

2. STUDY SITE

Kaloko-Honokohau National Historical Park has an area of 4.7 km^2, which includes numerous anchialine pools, two larger fishponds and coastal marine waters within the park's boundaries. Anchialine pools are enclosed bodies of water with an underground connection to the ocean and over half the known anchialine pools in the world are found in the Hawaiian Islands (NOAA, 2014 – <http://oceanservice.noaa.gov/facts/anchialine.html>) The park itself sits at the base of Hualalai Volcano (Figure 1). The "Hualalai Aquifer Sector Area" includes the entire Hualalai Volcano and is surrounded by Mauna Loa (Hawai'i County Plan, 2010). The marine and inland waters of the park and surrounding area are vital to the mission of KAHO, as they serve as natural habitats for six federally registered threatened or endangered species (National Park Service, 2013), as well as preserve traditional native Hawaiian aquaculture techniques. The main source of fresh groundwater recharge for these inland ecosystems is rainfall, though there is some additional contribution from fog drip and interception, irrigation runoff and wastewater discharge (National Park Service, 2013).

Climate on the Kona side of Hawai'i is much drier than the opposite side of the island; Hilo, receives on average more than 7800 millimeters of precipitation annually while Kona totals are much lower with an average of about 1500 millimeters per year (Giambelluca et al. 2013) (Figure 1). Generally, the Hawaiian Islands have two seasons: a wet, winter season from October to April and a relatively drier summer from May to September (Sanderson, 1993). In actuality, monthly climate normal precipitation totals for stations on the Kona side suggest winter months receive less precipitation with an average of 346 mm, compared to summer months with an average of 517 mm. Summer months also have larger variability in climate normal among individual

stations (Figure 2), this is due to the nature of seasonal precipitation, as localized convection is dominant in summer compared to cyclonic and frontal systems during winter (Sanderson, 1993).

The spatial precipitation patterns on the western side of the island are highly influenced by the topography of the region. The steep elevation gradient from the coast to the peak of Hualalai, and surrounded by Mauna Loa, results in a precipitation gradient with the amount of precipitation increasing with elevation from the coast to approximately 1500 meters and then decreasing further with elevation to the peak of Hualalai Volcano at approximately 2500 meters (Figure 1). As the recharge to Hualalai Aquifer is dependent on rainfall, the band of high precipitation is critical for maintaining freshwater resources for KAHO and surrounding sub-urban development and industry. High spatial variability is especially apparent in this band. For example, the Kalukalu 29.2 and Kanakemelai 29.5 stations, which are approximately 5 km apart but have opposite precipitation trends. Over the 30-year period from 1978 to 2007, Kalukalu has a significant decrease of -16.7 mm per year, while Kanakemelai has a slightly increasing trend of 0.3 mm per year, though not significant (Figure 3). To study the spatial trends over Hualalai Aquifer, four watersheds delineated by the State of Hawai'i Office of Planning (2014) were selected, including Kiholo, Keahole, Honokohau and Waiaha.

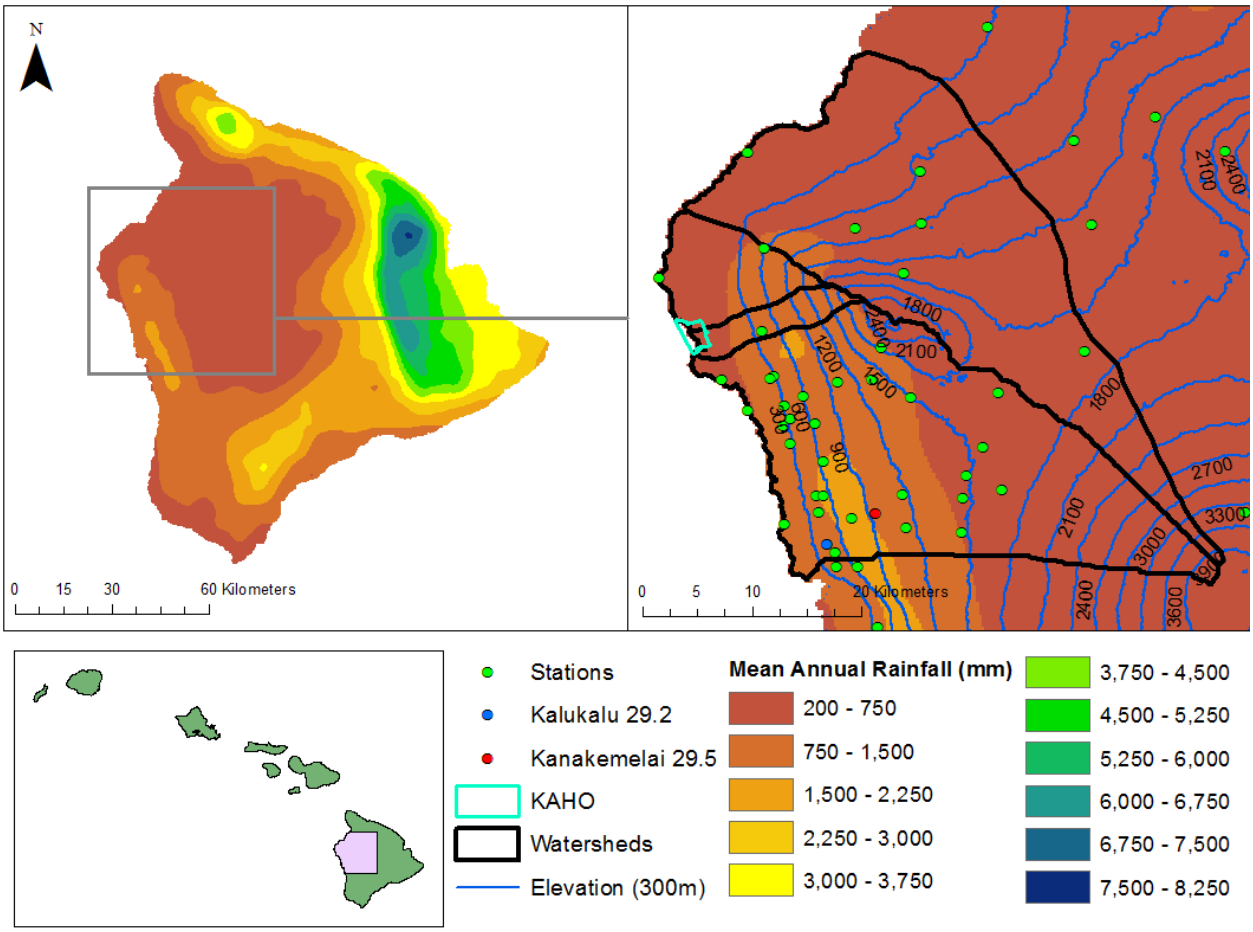

Figure 1. Site Map
Mean annual rainfall in mm between 1978-2007 from the Rainfall Atlas of Hawai'i (Giambelluca et al., 2007) for the island of Hawai'i. Fifty-five stations were selected within or around the four watersheds within the Hualalai Aquifer Sector. Kaloko-Honokohau National Historical Park (KAHO) extends from inland to the coastal waters.

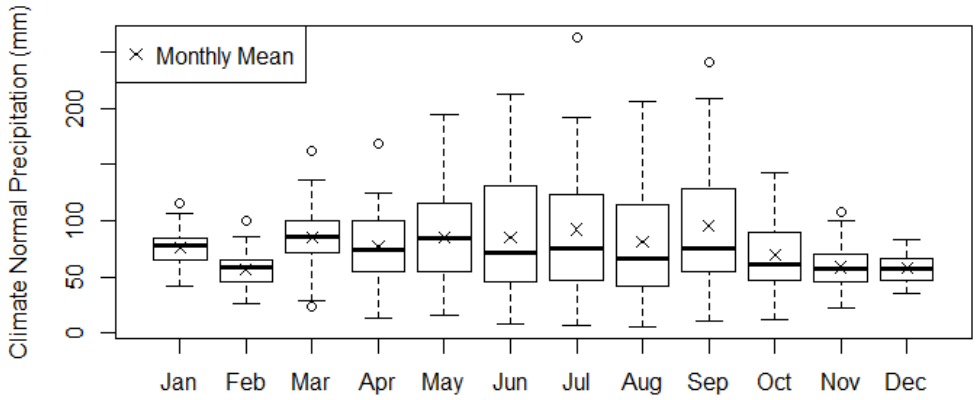

Figure 3. Monthly Climate Normals

Box and whisker plot of GIS-derived climate normal for each month based on the 55 selected stations. Boxes represent the lower and upper quartiles with the median value inside the box, whiskers represent the minimum and maximum values, though there are some outliers. Hawai'i typically has wetter winters compared to summer, however on the Kona side of the island, seasonal precipitation is the opposite. The summer seasons receives a slightly higher average precipitation and has increased variability in mean precipitation across the region.

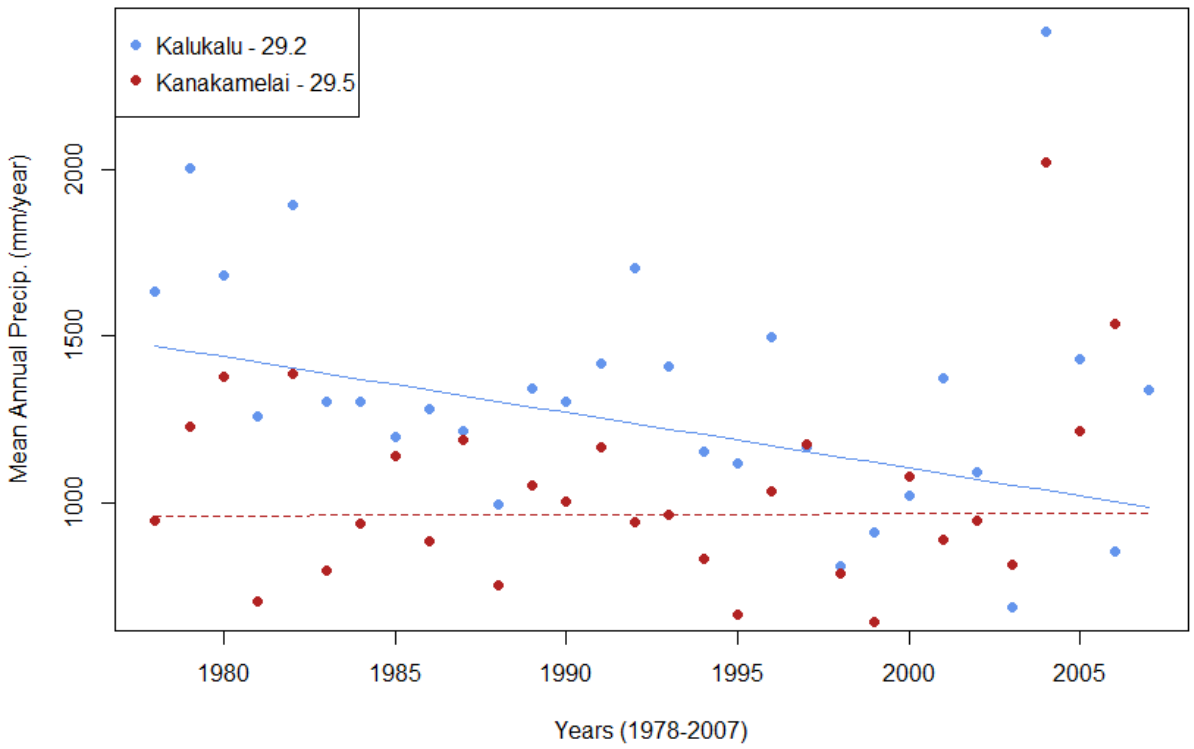

Figure 3. Time Series of Two Stations
Comparison of precipitation trends at two stations south of KAHO. Kalukalu 29.2 has a significant decreasing trend of -16.7 mm/year at the 5% level of significance. Kanakemelai has a slight increasing trend of 0.3 mm/year, though not significant.

3. METHODS

3.1 Data

Data were obtained from the University of Hawai'i at Manoa's Rainfall Atlas of Hawai'i (Giambelluca et al, 2013 <http://rainfall.geography.hawai'i.edu/>). Monthly precipitation totals and location for over 1000 stations on the Big Island in millimeters and the 30-year mean rainfall maps (both annual and monthly) were obtained from the Rainfall Atlas. The original spatial extent of these maps extended from 20.33 N to 18.85 N and 156.24 W to 154.67 W. Park boundary location and selected watersheds were obtained from the National Parks Service and the State of Hawai'i Office of Planning, respectively (<http://www.nps.gov/gis> and <http://planning.hawaii.gov/gis/>). All spatial data used the Geographic Coordinate System and World Geodetic System 1984 datum.

Hawai'i's history of plantation agriculture and need for monitoring water resources has resulted in one of the densest rain gauge networks in the world (Giambelluca et al, 1986). Station data were preprocessed to determine which station's records had a data record between the years of 1978-2007 and were within or surrounding the four study watersheds. The inclusion of stations surrounding the study watersheds was necessary for spatial interpolation. For each station, if the number of monthly records in a given year was complete (12 per year) then the annual precipitation was calculated by summing each month's observed precipitation. If at least 28 of the 30 years in the time period had a calculated annual precipitation, the station was used in the analysis; 55 stations within the approximately 4000 km^2 study area were used. (Appendix Table 1).

The climate normal for the 30-year period defined by the Rainfall Atlas was obtained for each point and used to calculate the average GIS-derived climate normal across the study area.

The average GIS-derived climate normal precipitation was 921 mm/year (Figure 3.) The station observation derived climate normal differed from the GIS-derived by -0.09%, therefore the GIS-derived normal was deemed sufficient for use.

3.2 Map Time Series

An annual adjustment factor was determined for each year to remove trends in precipitation due to various atmospheric oscillations that play a role in the Hawaiian climate, including the El-Niño Southern Oscillation (ENSO) and Pacific Decadal Oscillation (PDO) (Oki, 2004). This annual adjustment factor was equivalent to the ratio of the average precipitation for a given year ($\bar{P}_t$) and the average GIS-derived climate normal ($\bar{P}_{cn}$) (Table 1). The map of mean rainfall was multiplied by each annual adjustment factor ($\bar{P}_t / \bar{P}_{cn}$) spatially to create a series of 30 "Annually Adjusted Climate Normal" maps with the same spatial resolution and extent as the original mean rainfall map. The procedure is similar to the production of gridded temperature and precipitation datasets across the Continental United States by Hamlet and Lettenmaier (2005). Each station's climate normal ($P_{i,cn}$) was multiplied by the annual adjustment factor ($\bar{P}_t / \bar{P}_{cn}$) to yield an adjusted station value for each year ($P_{adj}{}_{i,t}$) to then be used in calculating residuals.

The residuals ($P_{r}{}_{i,t}$) were defined as the difference between the observed annual precipitation ($P_{i,t}$) and the adjusted value ($P_{adj}{}_{i,t}$) for a given station (Table 1). Each year's station residuals were then interpolated using inverse distance weighting (IDW) in R (R Core Team, 2014) with a power parameter of two. Since the model selection needed to fit a variogram for ordinary kriging cannot be easily automated without uncertainties (Fassnacht et al. 2003), IDW is an appropriate interpolation method for this procedure. A series of 30 "Interpolated Residual" maps was generated. The 55 selected stations formed the final spatial extent of the interpolated maps

and went from approximately 19.97° to 19.40° N and 156.06° to 155.45° W. Each year's Adjusted Climate Normal and Interpolated Residual map were then summed together to create 30 final "Time Series" maps to be used for statistical testing. These maps were approximately 250 meters in resolution.

3.3 Trend Analysis

The Mann-Kendall test is a non-parametric test and is widely used to detect monotonic upward or downward trend. The Sen's Slope estimate finds the associated rate of change of the Mann-Kendall trend. Once completed on an annual basis, the entire integrated spatial analysis was similarly done for each month in order to test for trends at the monthly timescale. The 30 "Time Series" maps were then stacked (Hijmans, 2014) on one another in R in order to perform the Mann-Kendall test for trend and Sen's Slope Estimation using the RKT Package (Marchetto, 2013). For each cell through the stack, the statistical tests were run through the time series and produced a unique output.

The rate and significance of change were also determined for each of the 55 station's time series using the Mann-Kendall test for trend and Sen's Slope estimate. The individual point time series were then interpolated using inverse distance weighting with a power parameter of two as per the prior residual interpolation, and ordinary kriging fitted to an exponential model. These statistical tests were done to compare the spatial differences in rate and significance of change between the integrated spatial analysis method and interpolation of point trends.

In addition to the Mann-Kendall and Sen's Slope tests, the Regional Kendall Test (RKT) was calculated over three different regions: these included the entire 55 stations in the study area, the 42 stations within the four selected watersheds, and 24 stations found in the middle elevations associated with the band of increased precipitation. The RKT was done to provide a more robust

analysis (Helsel and Frans, 2006) quantifying the rate of change over the entire region, rather than the individual station for comparison with the integrated spatial analysis.

To compare the calculated rates of change spatially with each method, the net volume of change was calculated for the total watershed area. The total watershed area is defined as the area of the four selected watersheds, not the entire spatial extent based on the station locations. The net volume of change is equal to the average rate of change within the total watershed area (m/yr) multiplied by the total watershed area (m^2). Similarly, the net volume of change was calculated within the watersheds, though only including the area that shows a significant trend.

Table 1. Data Schematic
Database format and equations used for determining the adjusted climate normal for a given year and the residuals between the observed station data and adjusted normal.

Station (1978...2007)	1,2,...,n	Average
Climate Normal (GIS)	$P_{i,cn}$	$\bar{P}_{cn}$
Station Data	$P_{i,t}$	$\bar{P}_t$
Adjusted Climate Normal	$P_{adj\,i,t} = \frac{\bar{P}_t}{\bar{P}_{cn}} \times P_{i,cn}$	$\frac{\bar{P}_t}{\bar{P}_{cn}}$
Residuals	$P_{Ri,t} = P_{i,t} - P_{adj\,i,t}$	$\lvert\bar{P}_R\rvert = \frac{\sum\lvert P_{Ri,t}\rvert}{n}$

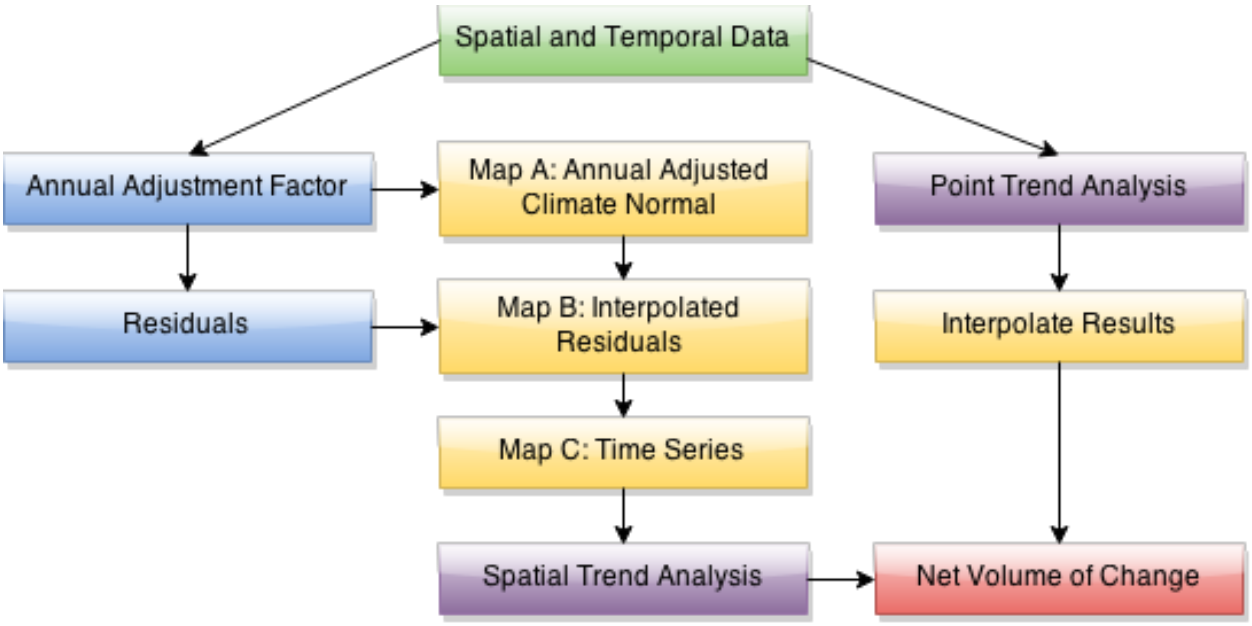

Figure 4. Flow chart of methodology
Comparison of methodology used for the integrated spatial analysis (left and center) and point trend analysis (right). The integrated spatial analysis first determines an annual adjustment factor and represents it spatially then calculates and interpolates residuals to create a spatial time series for statistical trend analysis. The point trend analysis begins with statistical testing of individual point trends which are then represented spatially. The calculated net volume of change is used to quantify results.

4. RESULTS

The annual IDW interpolation yielded a net volume decrease of -10.8 x 10^6 m^3/year (-7.98 mm/year) and ordinary kriging yielded -8.41 x 10^6 m^3/year (-6.20 mm/year) for the entire watershed area, IDW accounted for 129% of the total change determined by kriging. However, when comparing only significant areas, IDW results in a net volume decrease of only -0.639 x 10^6 m^3/year, compared to a decrease of -1.31 x 10^6 m^3/year for kriging. In this case, IDW only accounts for 49% of the total change determined by kriging. The spatial analysis resulted in only a -8.42 x 10^6 m^3/year (-6.27 mm/year) change, or 14% less for the entire watershed area. For the area of significant change, the integrated spatial analysis results in an annual change of -4.62 x 10^6 m^3/year, or nearly seven times more than IDW or 3.5 times more than kriging (Figure 5a.)

At the monthly time scale, the interpolated point trends result in a larger deficit than the integrated spatial analysis when the entire watershed area is considered, similar to the annual net volume results (Figure 5b.). However, when only significant areas are considered, the integrated spatial analysis results in a much larger deficit in net volume entering the aquifer system. Both methods resulted in no significant change in net volume for the months of January and February. All months have a similar positive or negative monthly trend between the two methods.

Seasonally, during the summer months (April-September for this analysis) there is a general negative trend in the net volume of change, except June where there is nearly no net change over the 30-year time period. During the cooler months (October-March) there is an overall positive trend in the net volume of change (excluding December). However that the largest net volume increase that occurs in the cooler months is +10.6 x 10^6 m^3/year in March, from the spatial analysis method, regardless of significance, is only half the largest decrease of -25.3x 10^6 m^3/year

occurring in May. On average, the integrated spatial analysis method resulted in a -15.9 x 10^6 m^3/year net volume of change between April-September and only a +1.2 x 10^6 m^3/year net volume of change between October-March.

The Z_τ values calculated by the Regional Kendall Test are -1.420 for the entire 55 stations, -1.537 for the 42 stations within the four selected watersheds and -2.430 for the 24 stations in the middle-elevations that correspond with the band of highest precipitation. At the α=0.05 significance level, the first two regions do not show a significant regional trend, however the middle-elevation regions has a median significant decreasing trend of -3.8 x10^6 m^3/year (-14.01 mm over an area of approximately 271 km^2 annually). It can be noted that at the α=0.1 significance level all trends are significant and continue to reflect an overall decrease in annual precipitation.

The map characteristics produced by the integrated spatial analysis show more detail in the spatial pattern of change (Figure 6.) This is seen in the elongated region of significance extending from the coast to above the middle elevations and includes a majority of the middle elevation-high precipitation rain band when compared to the region of significance produced from IDW interpolation. Similarly, larger areas of the highest rates of change are produced by the integrated spatial analysis, as opposed to circular bullseyes centered around stations with the highest trends.

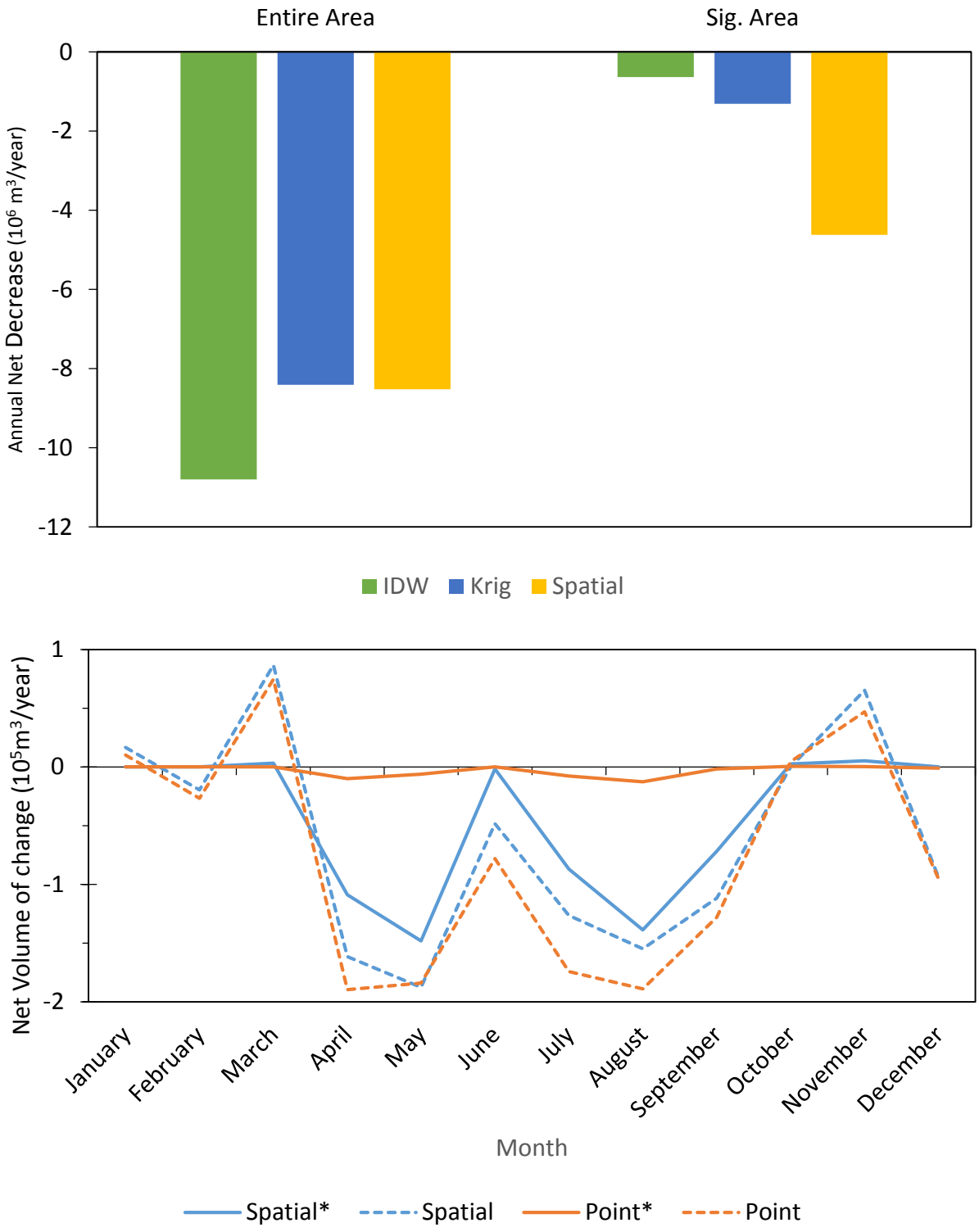

Figure 5. Net Volume Calculations
Top – annual net volume decrease calculated by the interpolation of point trends with IDW and ordinary kriging, and the integrated spatial analysis method. Bottom – monthly net volume of change as calculated by IDW interpolation and the integrated spatial method. This includes values for both the entire watershed area and only those with a significant trend (denoted by *).

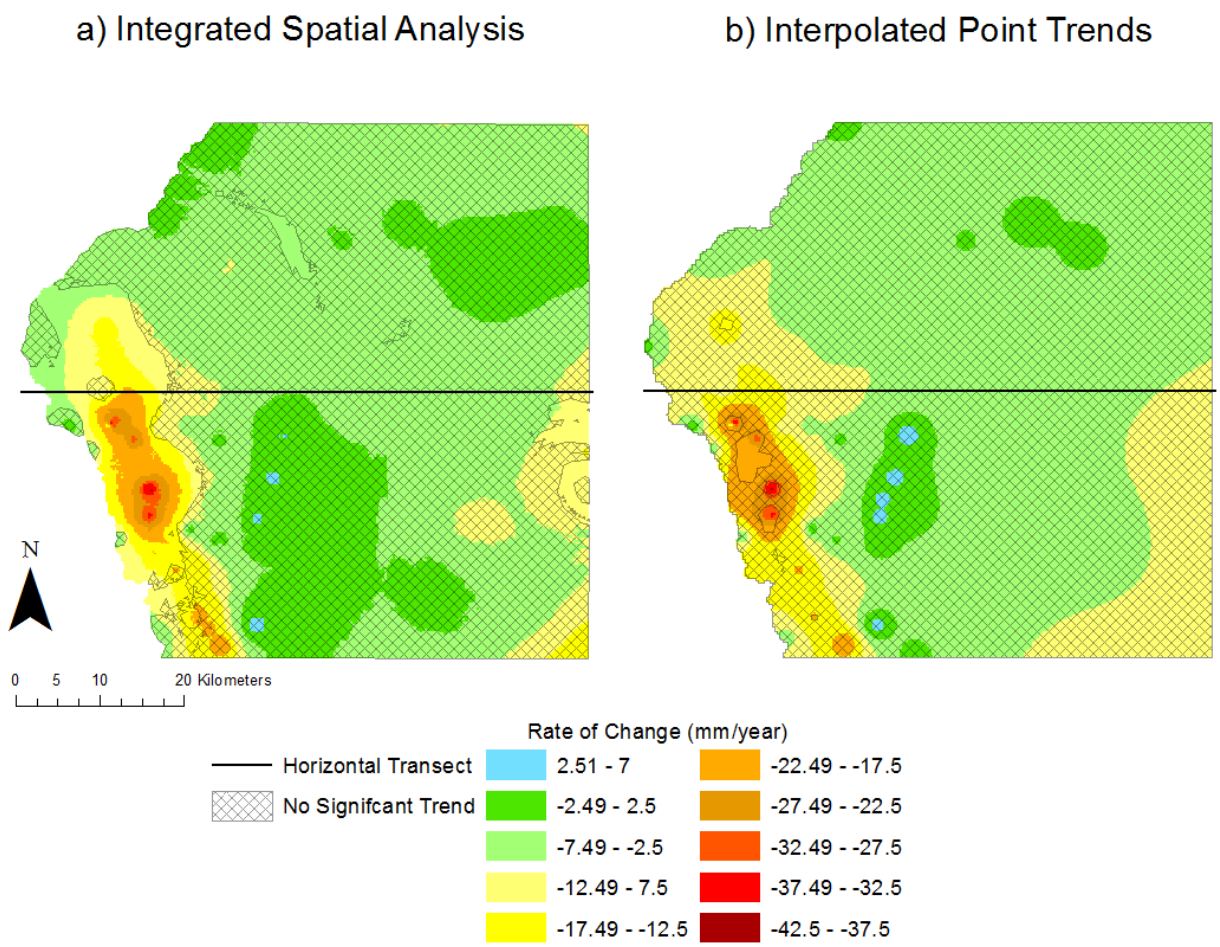

Figure 6. Annual Comparison Maps
Visual comparison of annual1 results from a) integrated spatial analysis and b) IDW. Cross-hatched areas indicate no significant trend determined. The horizontal transect (Figure 7) intersects Kaloko-Honokohau National Historical Park and near the peak of Hualalai Volcano.

5. DISCUSSION

The map characteristics produced by the integrated spatial analysis show more detail in the spatial pattern of change (Figure 6). This is seen by the elongated region of significant change that extends from the coast to higher elevations beyond the high precipitation band, compared to isolated circular regions produced by IDW interpolation. Similarly, larger areas of the highest rates of change (approximately 20 mm per year and up) are produced by the integrated spatial analysis as opposed to bullseyes centered at stations with the highest observed trends. Greater detail can also be seen in the transect from KAHO upslope through Hualalai Volcano (Figure 7b.) as the integrated spatial analysis produces more localized maxima/minima.

The integrated spatial analysis method is able to account for both spatial and temporal variability in time series data, resulting in a more accurate representation of spatial trends and calculated net volume of change. Temporal inhomogeneities can, and often, exist in precipitation time series for numerous reasons, including atmospheric oscillations and inconsistent observation location (Hamlet and Lettenmaier. 2005). Consistent observation locations are important in maintaining the representativeness of a station for a particular topographic location; if observations are taken at multiple locations with varying topography for a single station, there is the potential that trends are resultant of the change in location to a different precipitation regime rather than a change in climatic trends. These inhomogeneities can result in a strong bias when used for either temporal or spatial analysis, and merit the use of temporal adjustments to account for potential bias (Hamlet and Lettenmaier, 2005). By determining the annual adjustment factor and calculating the residual between the adjusted climate normal and observations, the integrated spatial analysis effectively accounts for seasonal and decadal variability and yields a temporally adjusted time

series. Temporal adjustments account for long-term trends while residual interpolation by inverse distance weighting creates a continuous surface and maintains as much spatial information as possible. This is especially valuable in the dense rain gauge network found in western Hawai'i.

Single station trends are often assumed to be representative of a region as a whole, especially in regions with limited climate observations. However, since the integrated spatial analysis considers change on a pixel by pixel basis, it allows for a more complete assessment of trends in a region as spatial variability can occur at multiple spatial scales within the region itself. Often, overall regional trends are not portrayed due to smaller local variation or vice versa where local variation is masked by a larger scale trend (Pielke et al. 2002). This local variability is exemplified by the two stations Kalukalu and Kanakamelai (Figures 1 and 3). While annual precipitation typically increases with elevation, Kalukalu is closer to the coast and receives more precipitation in most years than Kanakamelai. These two stations also have opposite trends even though they are in relatively close proximity. If either station was solely used to be representative of the entire region, or even the middle band of higher precipitation, resulting assumptions would be inaccurate for the highly variable region.

RKT results also demonstrate the large spatial variability in the region; no significant trend was detected when the region considered all 55 stations or those stations within the Hualalai Aquifer watersheds boundaries, but the 24 stations concentrated closest to the highest precipitation band had a significant decrease of over 14 mm per year. The lack of a significant trend across the entire 55 station area and entire Hualalai Aquifer watersheds boundary suggest the overall trend is masked due to differing trends taking place at smaller scales within the region.

The length of a station record can influence the significance and rate and significance of a regional trend. Naturally occurring climate oscillations with long-term variability can result in

biased assessment of temporal trends if the length of data record is not sufficiently longer than the phase of cyclical component (Chen and Grasby, 2009). In order to avoid this, a time series should be at least longer than one-phase of the cycle length and ideally greater than three phase lengths (Chen and Grasby, 2009). Longer length records have also been noted to be associated with a higher level of significance when compared with shorter record periods for a similar region (Venable et al. 2012). This suggests that a shorter station record may bias the significance of a trend in a region depending on the phase of cycle that the record takes place in and all records used should be of comparable length.

By ensuring that all stations had at least 28 of 30 complete years available to determine the adjusted climate normal, the integrated spatial analysis limits the effects that differing station record length may have on significance for this 30-year period. Similarly, a 30-year record is considered to be the amount of years required to determine an appropriate climate normal (International Meteorological Vocabulary, WMO – No. 182). While the phase of PDO is variable and often multi-decadal, the period from the mid 1970's to mid 2000's experienced one phase length from negative early in the time period, to quickly becoming positive and then back to negative before the end of the time period (JISAO, 2014). Oscillations due to ENSO are of much smaller length, ranging from 18 months to 6 years on average (JISAO, 2014) so the selected time period will have a minimal bias. Coincidentally, KAHO was established in 1978 and 1978-2007 is the time period in which the most recent version of the Hawai'i Rainfall Atlas (Giambelluca et al. 2013) is available. This enables the integrated spatial analysis to assess change in the net volume entering Hualalai Aquifer since conservation efforts with KAHO began.

The decrease in net volume of precipitation entering the aquifer during the time period, regardless of analysis method, implies an overall drying pattern in Western Hawai'i (Figure 5).

The areas with the largest decreases in annual precipitation are the middle elevation band with the highest precipitation, with values as high as 37 mm/year (Figure 6). Along a transect directly west from KAHO to near the peak of Hualalai Volcano, the maximum decrease from the integrated spatial analysis is approximately 19 mm/year, which also falls in the high-precipitation band in the middle elevations (Figure 7.) There is seasonality with the net volume of water entering the aquifer as the drier, cool months have seen a slight increase, while the overall trend is a net decrease.

There are limited studies of climate change specifically in Western Hawai'i, but these results do agree with some of the previous findings for the Big Island. Changes in the frequency of extreme precipitation events on all of the Hawaiian Islands vary depending on location: the Hilo side of Hawai'i has generally seen an increase in precipitation intensity, in addition to a significant positive trend centered around Mauna Loa in the center of the island. In contrast, the Kona region has a negative trend (Chu et al., 2010). The overall reduction in moderate and high intensity precipitation events in Kona, which are considered to be extreme, yields fewer days with precipitation and therefore lower precipitation amounts. While the integrated spatial analysis does not include precipitation intensity, the high elevations, including Mauna Loa, are part of the limited regions in which the annual rate of change is near zero and agree with the positive trend in extreme precipitation frequency observed there. It is important to note that these results however are not statistically significant for either the integrated spatial analysis or interpolated point trends for the majority of the study area surrounding Kona, decreasing precipitation trends also agree with the negative trend in extreme precipitation events. Spatial variability in terms of precipitation intensity is seen across the Hawaiian Islands, with negative trends observed in Oahu and Maui, also opposite to the overall positive trend seen on the Island of Hawai'i (Chen and Chu, 2014). Though both methods of analysis successfully picked up on these annual trends, the integrated spatial analysis

greatly outperforms interpolation when considering seasonal and statistically significant trends (Figure 5).

The net volume calculated from the integrated spatial analysis can be compared with values calculated from interpolation by inverse distance weighting and ordinary kriging. At the annual time scale and when considering all trends, ordinary kriging results in nearly the same change in net volume as the integrated spatial analysis, while inverse distance weighting overestimates (Figure 5a). Though this may suggest ordinary kriging is a comparable, and potentially simpler, method of spatial analysis, resulting values of net volume with only significant areas considered are inconsistent as both interpolation methods underestimate net volume.

Varying results between methods indicate the limitations of inverse distance weighting and ordinary kriging. Inverse distance weighting is a widely used and accepted method of interpolation, particularly for use with precipitation for short storm-duration time periods to much longer climatic time-scales. The ability to determine the control parameter that is best suited for the surface to be interpolated also makes IDW a suitable method of spatial interpolation (Chen and Liu, 2012). Ordinary kriging often results in a more detailed interpolation surface, limiting the appearance of "bullseye" trends that are artifacts of inverse distance weighting (Soenario et al., 2010), in doing so however, the interpolation process is more complex. The statistical model needed to fit the variogram for interpolation is not always clear, making automation of the process difficult and computationally ineffective (Fassnacht et al, 2003). Due to the inconsistent results and complicated processes needed for ordinary kriging, it makes sense and is more efficient to automate the interpolation of residuals in the integrated spatial analysis with inverse distance weighting. Regardless of the interpolation method used within the integrated spatial analysis, the overall result

is more accurate given the realistic numbers for net volume of change at the monthly time scale and the more continuous map surface of annual rate of change that is created.

While the time series map created for each year from 1978-2007 does provide an overall realistic portrayal of precipitation for a given time there will still be some variation between the adjusted time series and what actually occurred. For January and July, adjusted precipitation values are slighlty less than the observed precipitation for 27 additional stations within the study area that did not meet the criteria needed for inclusion in the integrated spatial analysis (Figure 8.). R^2 values of 0.46 and 0.56 for January and July, respectively, suggest that the calculated precipitation matches observations roughly half of the time. The mean absolute error calculated among all 27 stations for the 30 years is 30.82 mm for January and 33.79 mm for July. Variation between the calculated and observed precipitation increases as observed precipitation values at a given station increases. The Breush-Pagan test for heteroscedasticity (Breush and Pagan, 1979) was done in R (Zeileis and Hothorn, 2002) for the linear models produced with the January and July data and the residuals do exhibit statistically significant heteroscedasticity. This suggests that future implementation of the integrated spatial analysis could be improved; which can be done by increasing the number of stations used to calculate the annual adjustment factor or calibrating this value based on a linear model. It is important to note that the additional 27 stations not included in the integrated spatial analysis contain incomplete or otherwise flawed data and the overall decreasing results from the integrated spatial analysis are still deemed realistic.

There are several observed atmospheric changes that have taken place and are likely to play a role in the decrease in precipitation across the Kona Region, as well as the entire island chain. Hawai'i's climate has largely been driven by both ENSO and PDO (Chu and Chen, 2005). During El-Niño events and when ENSO neutral, Hawai'i is typically drier, while wet during La

Nina events (Chu and Chen, 2005). Significant negative correlation between Hawaiian rainfall and PDO has also been observed, suggesting warm phase (positive) PDO is associated with less precipitation and cold phase (negative) PDO with increased precipitation (Chu and Chen, 2005). The decades from the mid-1970's to early 2000's are associated with an "epoch of low rainfall" linked with a positive PDO trend (Chu and Chen, 2005). However, observed temperature trends in Hawai'i that were once tightly coupled with PDO are beginning to diverge from PDO (and therefore ENSO) trends in favor of increasing influence of climate change and an overall warming of global air temperature (Giambelluca et al. 2008). While these shifting trends have only been reported for temperature, it is safe to assume a similar shift from ENSO/PDO trends to global warming trends is capable for Hawaiian precipitation. This suggests the already low annual precipitation observed in the recent decades due to warm (positive) PDO phase could be further enhanced by drying across the islands due to climate change.

A dominant control in the local weather, especially as elevation increases, is the occurrence of the Trade Wind Inversion (TWI). The TWI acts to inhibit large-scale vertical motion, only allowing shallow cloud development below the inversion itself, resulting in dry conditions. A climatological study of inversion variability indicates that the TWI is present over 80% of the time on the Hilo side of Hawai'i (Cao et al. 2006). Radiosonde data used to detect the presence of the TWI does not exist for Kona, but similar percent occurrence has been observed at Lihu'e on Kauai and suggests 80% occurrence can be generalized across the island chain. Variability in inversion height is more likely across the Big Island and is in large part associated with topographic differences. While trends in occurrence are connected to ENSO and are likely representative of warm phase PDO, should climate change continue to increase the frequency of occurrence, Hawaiian climate will continue to dry (Cao et al. 2006).

Continued decrease in precipitation entering the Hualalai Aquifer Sector Area has the potential for long-term implications for water resource management. The Kona Region is already water limited compared to other parts of the islands with significantly less precipitation on average. While there is generally no overland flow on the Kona side to measure streamflow, observed decreasing trends in baseflow on neighboring islands support an overall decrease in water availability from rainfall (Bassiouni and Oki, 2013), having lasting effects on runoff, and more importantly for Kona, recharge. Stable isotope samples of fresh groundwater near the coast strongly suggest recharge at least partially originates from high-altitude groundwater (Tillman et al., 2014) as opposed to localized precipitation. Kona itself has a large and growing tourism industry and is the government and industrial center for Western Hawai'i. Increased population growth and development has increased demand and competition for water supplies (Hawai'i County Water Use and Development Plan, 2010). KAHO is also dependent on groundwater, with 25-70% of freshwater derived from high level groundwater (Tillman et al., 2014), as conservation of the numerous anchialine pools and fishponds is a main mission of the park.

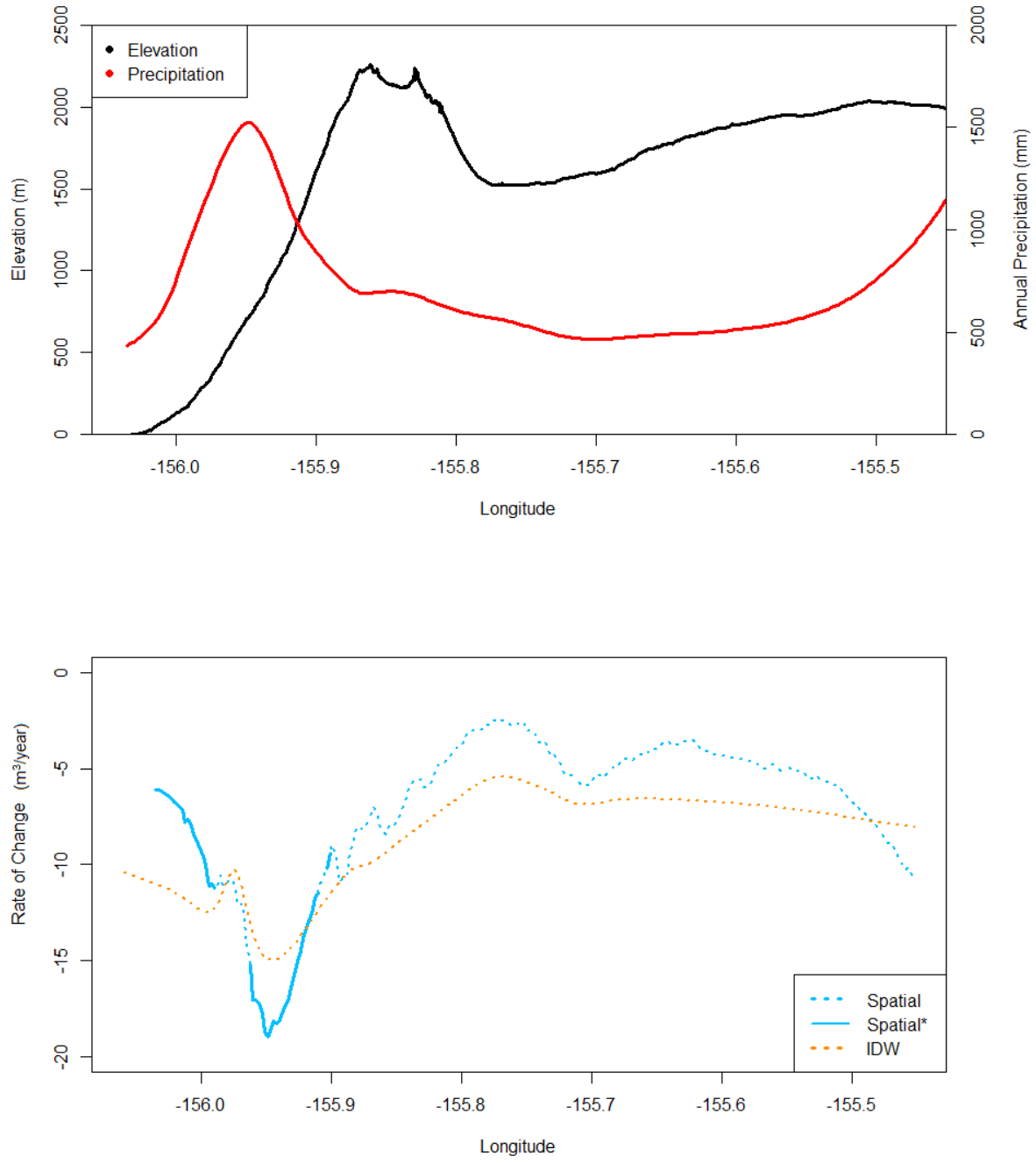

Figure 7. Horizontal Transects
Horizontal transects extending from Kaloko-Honokohau National Historical Park across the study area (19.68° N,-156.06° W) to (19.68°W,-155.45° W) (a) Elevation and annual precipitation (b) rate of change from the integrated spatial analysis and IDW interpolation, there was no significant change along the IDW produced transect.

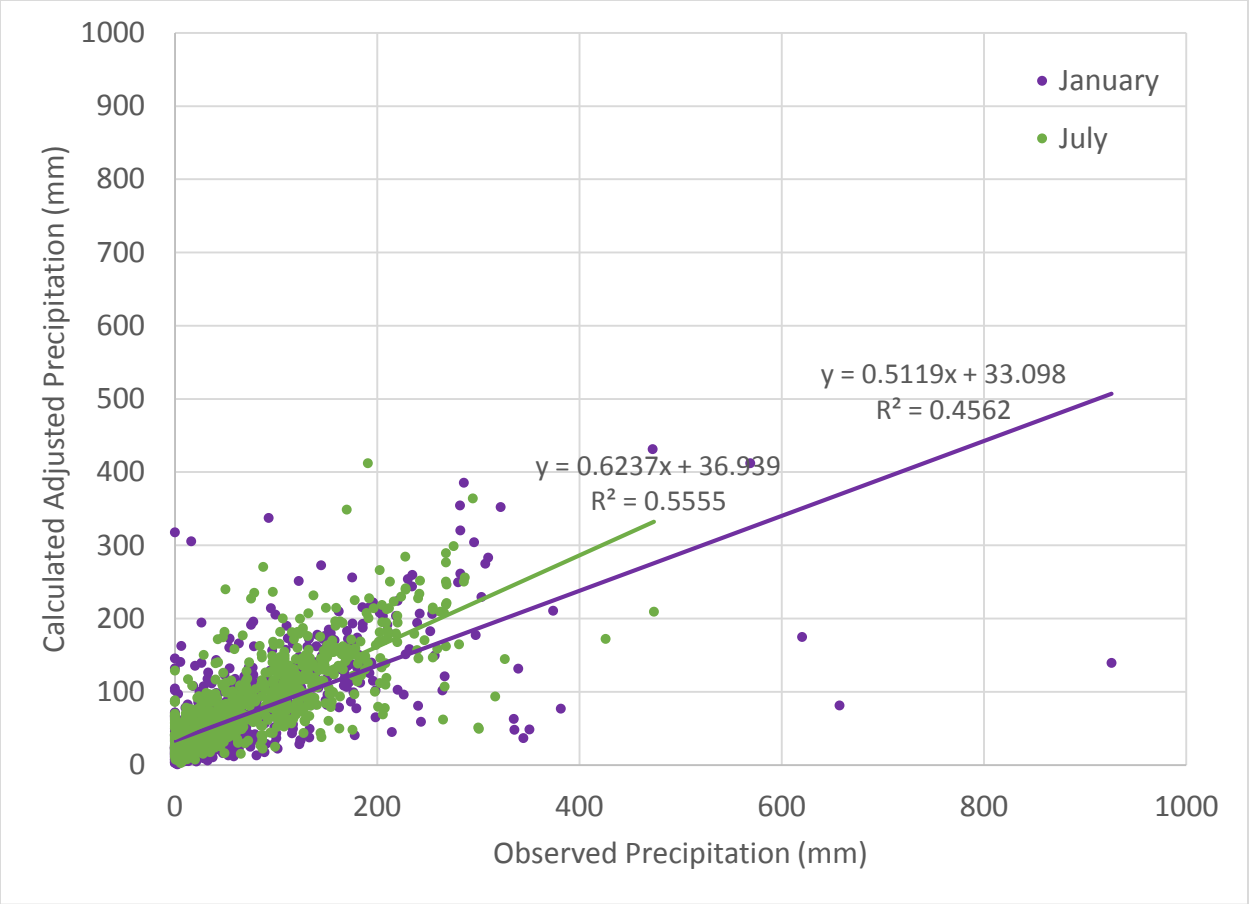

Figure 8. Observed versus Calculated Precipitation – January and July
Observed precipitation at 27 point stations within the study area that were not included in the integrated spatial analysis versus the calculated precipitation at each station based on the adjusted time series.

6. CONCLUSIONS

Precipitation trends on the Kona Side of Hawai'i surrounding KAHO are highly variable in both space and time. The number of differing climatic zones in a relatively small area result in spatial precipitation patterns that generally follow the western slope of Hualalai and Mauna Loa volcanoes. The greatest precipitation amounts, of about 2000 mm per year, are seen in the middle elevations and decreasing to around 200 mm per year at the coast and higher elevations. Over the 30-year time period from 1978-2007, mean annual precipitation has been decreasing at rates as high as 37 mm/year. The timing of greatest rainfall appears to be shifting, as the wet summer season is getting significantly drier while the dry winters are receiving slightly more rain, resulting in an overall decrease in mean annual precipitation. The regions that receive the greatest rainfall are also shifting, as the wet middle-band of precipitation is significantly drying, while high elevations near the peaks are not changing or slightly increasing. This spatial pattern results in an overall decrease in the mean annual precipitation and an associated decrease in water entering the Hualalai Aquifer system.

The new method of spatial analysis provides an improved assessment of these changes compared to the inverse distance weighting or ordinary kriging of point trends, as well the Regional Kendall Test that combines point stations. This new method could be useful in analyzing spatial trends in a number of regions around the world and help in understanding the changes in water resources across a region. While it is not limited to precipitation analysis, its implementation outside the Kona Region of Western Hawai'i could broaden the limited understanding of precipitation trends across the globe, especially those that are water limited.

7. REFERENCES

Bassiouni, M., & Oki, D. S. (2013). Trends and shifts in streamflow in Hawai'i, 1913-2008. *Hydrological Processes*, *27*(10), 1484–1500. doi:10.1002/hyp.9298

Bivand, R., Keitt, T., Rowlingson, B. (2014). Rgdal: Bindings for the Geospatial Data Abstraction Library. R package version 0.8-16. http://CRAN.R-project.org/package=rgdal.

Brekke, L. D., Kiang, J. E., Olsen, J. R., Pulwarty, R. S., Raff, D. A., Turnipseed, D. P., Webb , R. S., White, K. D. (2009). *Climate Change and Water Resources Management : A Federal Perspective*. Circular 1331 U.S. Department of the Interior, U.S. Geological Survey.

Breush, T., & Pagan, P. (1979). A Simple Test for Heteroscedasticity and Random Coefficient Variation. *Econometrica 47(5).* 1287-1294. doi: 10.2307/1911963

Cao, G., Giambelluca, T. W., Stevens, D. E., & Schroeder, T. a. (2007). Inversion Variability in the Hawaiian Trade Wind Regime. *Journal of Climate*, *20*(7), 1145–1160. doi:10.1175/JCLI4033.1

Chen, F.-W., & Liu, C.-W. (2012). Estimation of the spatial rainfall distribution using inverse distance weighting (IDW) in the middle of Taiwan. *Paddy and Water Environment*, *10*(3), 209–222. doi:10.1007/s10333-012-0319-1

Chen, Y. R., & Chu, P.-S. (2014). Trends in precipitation extremes and return levels in the Hawaiian Islands under a changing climate. *International Journal of Climatology*, doi:10.1002/joc.3950

Chen, Z., & Grasby, S. E. (2009). Impact of decadal and century-scale oscillations on hydroclimate trend analyses. *Journal of Hydrology*, *365*(1-2), 122–133. doi:10.1016/j.jhydrol.2008.11.031

Chu, P.-S., & Chen, H. (2005). Interannual and Interdecadal Rainfall Variations in the Hawaiian Islands*. *Journal of Climate*, *18*(22), 4796–4813. doi:10.1175/JCLI3578.1

Chu, P.-S., Chen, Y. R., & Schroeder, T. a. (2010). Changes in Precipitation Extremes in the Hawaiian Islands in a Warming Climate. *Journal of Climate*, *23*(18), 4881–4900. doi:10.1175/2010JCLI3484.1

Clow, D. W. (2010). Changes in the Timing of Snowmelt and Streamflow in Colorado: A Response to Recent Warming. *Journal of Climate*, *23*(9), 2293–2306. doi:10.1175/2009JCLI2951.1

Daly, C., Halbleib, M., Smith, J. I., Gibson, W. P., Doggett, M. K., Taylor, G. H., & Pasteris, P. P. (2008). Physiographically sensitive mapping of climatological temperature and

precipitation across the conterminous United States. *International Journal of Climatology*. doi:10.1002/joc

Department of Water Supply, County of Hawaii. (2010). *Hawaii County Water Use and Development Plan Update - Hawaii Water Plan.* Funkunga & Associates, Inc. (Vol. 96814).

Engott, J. A. (2011). A Water-Budget Model and Assessment of Groundwater Recharge for the Island of Hawai ‘ i. *USGS Scientific Investigations Report 2011-5078.* (pp. 1–53).

Falkland, A. (1999). Tropical island hydrology and water resources: Current knowledge and future needs. Paper presented. *2nd International Colloquium on Hydrology and Water Management in the Humid Tropics*. Panama, Rep. of Panama. UNESCO-IHP. 22-26 March, 1999.

Fassnacht, S. R., Dressler, K. A., & Bales, R. C. (2003). Snow water equivalent interpolation for the Colorado River Basin from snow telemetry (SNOTEL) data. *Water Resources Research*, *39*(8). doi:10.1029/2002WR001512

Giambelluca, T.W., Q. Chen, A.G. Frazier, J.P. Price, Y.-L. Chen, P.-S. Chu, J.K. Eischeid, and D.M. Delparte, 2013: Online Rainfall Atlas of Hawai'i. *Bull. Amer. Meteor. Soc.* 94, 313-316, doi: 10.1175/BAMS-D-11-00228.1.

Giambelluca, T. W., Diaz, H. F., & Luke, M. S. a. (2008). Secular temperature changes in Hawai'i. *Geophysical Research Letters*, *35*(12), L12702. doi:10.1029/2008GL034377

Giambelluca, T. W., Nullet, M. A., & Schroeder, T. A. (1986). Rainfall Atlas of Hawai'i. Water Resources Research Center and Department of Meteorology, University of Hawaii at Manoa.

Hamlet, Alan F. Lettenmaier, D. P. (2005). Production of Temporally Consistent Gridded Precipitation and Temperature Fields for the Continental United States *. *Journal of Hydrometeorology*, *6*, 330–336.

Helsel, B. D. R., & Hirsch, R. M. (1992). Statistical Methods in Water Resources. *Techniques of Water-Resources Investigations of the United States Geological Survey. Book 4, Hydrologic Analysis and Interpretation.* Ch. A3.

Helsel, D. R., & Frans, L. M. (2006). Regional Kendall test for trend. *Environmental Science & Technology*, *40*(13), 4066–73.

Hijmans, R.J., (2014) raster: Geographic data analysis and modeling. R package version 2.2-31. http://CRAN.R.project.org/package=raster

IPCC, 2013: Climate Change 2013: The Physical Science Basis. Contribution of Working Group I to the Fifth Assessment Report of the Intergovernmental Panel on Climate Change [Stocker, T.F., D. Qin, G.-K. Plattner, M. Tignor, S.K. Allen, J. Boschung, A. Nauels, Y.

Xia, V. Bex and P.M. Midgley (eds.)]. Cambridge University Press, Cambridge, United Kingdom and New York, NY, USA, 1535 pp, doi:10.1017/CBO9781107415324.

Joint Institute for the Study of the Atmosphere and Ocean. (2014). The Pacific Decadal Oscillation (PDO). [Available online at http://jisao.washington.edu/pdo/]

Leong, J., Marra, J.J., and Coauthors (2013). Ch. 23 Hawai'i and U.S. Affiliated Pacific Islands. *Climate Assessment Report – Draft for Public Climate.* v. 11 Jan 2013

Marchetto, A. (2014). Rkt: Mann-Kendall test, Seasonal and Regional Kendall Tests. R package version 1.3. http://CRAN.R-project.org/package=rkt

National Park Service (2014). Geography and Mapping Technologies, Geographic Information Systems. [Available online at http://www.nps.gov/gis/]

National Park Service (2013). Kaloko-Honokohau Cultural Center Environmental Assessment. U.S. Department of the Interior, Kaloko-Honokohau National Historical Park, Hawai'i.

NOAA (2014). What is an anchialine pool? [Available online at http://oceanservice.noaa.gov/facts/anchialine.html]

Nullet, D., & Ekern, P. C. (1988). Temperature and insolation trends in Hawaii. *Theoretical and Applied Climatology*, *39*(2), 90–92. doi:10.1007/BF00866393

Oki, D. S. (2004). Trends in streamflow characteristics at long-term gaging stations, Hawaii. *U.S. Geological Survey Scientific Investigations Report 2004-5080*, 120.

Pebesma, E.J. (2004). Multivariable geostatistics in S: the gstat package. Computers & Geosciences, 30: 683-691.

Pebesma. E.J. & Bivand, R.S. (2005) Classes and methods for spatial data in R. R News 5 (2), http://cran.r-project.org/docs/Rnews./

Pielke Sr., R. A., and Coauthors (2002). Problems in evaluating regional and local trends in temperature: an example from eastern Colorado, USA. *International Journal of Climatology*, *22*(4), 421–434. doi:10.1002/joc.706

R Core Team (2014). R: A language and environment for statistical computing. R Foundation for Statistical Computing, Vienna, Austria. http://www.R-project.org/.

Sanderson, M. (1993). *Prevailing Trade Winds, Weather and Climate in Hawai'i.* University of Hawai'i Press: Honolulu.

Safeeq, M., Mair, A., & Fares, A. (2013). Temporal and spatial trends in air temperature on the Island of Oahu, Hawaii. *International Journal of Climatology*, *33*(13), 2816–2835. doi:10.1002/joc.3629

Soenario, I., Plieger, M., Sluiter, R. (2010). Optimization of Rainfall Interpolation. *Koninklijk Nederlands Meteorolgisch Instituut (KMNI) Internal Report 2010-01*.

Stabler, B. (2013). Shapefiles: Read and Write ESRI Shapfiles. R package version 0.7. http://CRAN.R-project.org/package=shapefiles

State of Hawaii Office of Planning. (2014). Hawaii Statewide GIS Program. [Available at http://planning.hawaii.gov/gis/]

Timm, O., & Diaz, H. F. (2009). Synoptic-Statistical Approach to Regional Downscaling of IPCC Twenty-First-Century Climate Projections: Seasonal Rainfall over the Hawaiian Islands*. *Journal of Climate*, *22*(16), 4261–4280. doi:10.1175/2009JCLI2833.1

Venable, N. B. H., Fassnacht, S. R., Adyabadam, G., Tumenjargal, S., Fernández-Giménez, M., & Batbuyan, B. (2012). Does the length of station record influence the warming trend that is perceived by mongolian herders near the Khangai Mountains? *Pirineos*, *167*, 69–86. doi:10.3989/Pirineos.2012.167004

Zeileis, A., & Hothorn, T. (2002). Diagnostic Checking in Regression Relationships. R News 2(3), 7-10. http://CRAN.R-project.org/doc/Rnews/.

APPENDIX

Table A1. Station information and metdata of 55 stations used in integrated spatial analysis and point trend analysis.

Station Number	Name	Latitude (decimal degrees)	Longitude (decimal degrees)	Elevation (meters)	Observer	Data Source	Station Status	Mean Annual Rainfall (mm)
26	Takashiba	19.49	-155.9	640.24	KONA EXP STATION	NRFill, State	Discontinued	1612.29
26.2	Kealakekua	19.49	-155.91	442.07	GREENWELL ESTATE	Fill, NCDC, State, State/NCDC	Current	1252.69
27	Honaunau	19.44	-155.88	332.32	TANAKA S	Fill, NCDC, NRFill, State, State/NCDC	Current	1318.43
27.4	City Of Refuge	19.42	-155.91	4.57	HAW NATL HSTL PA	Fill, NCDC, State, State/NCDC	Current	717.83
29.2	Kalukalu	19.51	-155.92	457.32	GREENWELL EC	NRFill, State	Discontinued	1307.07
29.5	Kanakamelai	19.53	-155.88	951.22	WH GREENWELL ESTATE	Fill, State	Discontinued	1357.02
29.8	Onouli (1600)	19.5	-155.91	487.8	GREENWELL ESTATE	Fill, State	Discontinued	1324.26
30	Komakawai	19.4	-155.77	1875	MCCANDLESS RANCH	NRFill, State	Discontinued	698.06
30.3	Kiilae Stream	19.41	-155.85	883.54	USGS	NRFill, State	Discontinued	1990.31
31	Haupuu	19.43	-155.81	1371.95	MCCANDLESS RANCH	NRFill, State	Discontinued	938.23
39	Mauna Lo Slo Obs	19.54	-155.58	3397.87	NWS	Fill, NCDC, State/NCDC	Current	452.08
68.13	Keahole Airport	19.73	-156.06	3.05	FAA-HAWN AIRLINE	Fill, NCDC, NRFill, State, State/NCDC	Current	329.43
68.16	Holualoa-Stecker	19.61	-155.96	233.23	STECKER H C	NRFill, State	Discontinued	1005.78

68.3	Kona Airport	19.64	-156.01	4.57	HAWN AIRLINES	Fill, NCDC, NRFill, State, State/NCDC	Discontinued	575.33
69.16	Holualoa Makai	19.62	-155.96	317.07	WEINRICH SID	NRFill, State	Discontinued	1035.69
69.23	Kona Sunshine Es	19.59	-155.95	274.39	NICHOLS R C	NRFill, State	Discontinued	1013.42
69.3	Honokohau Ranch	19.68	-155.97	388.72	GREENWELL EC	Fill, NRFill, State	Discontinued	1230.03
69.5	Kaiolu	19.62	-155.99	9.15	JC TYLER SR	NRFill, State	Discontinued	719.43
69.7	Kailua-Yowell	19.65	-155.96	289.63	YOWELL WS	Fill, State	Discontinued	1151.79
69.9	Keopu Mcwayne	19.65	-155.97	243.9	PUUWAAWAA RANCH	NRFill, State	Discontinued	1058.3
70.1	Halepiula Shed	19.73	-155.86	1371.95	PUUWAAWAA RANCH	Fill, State	Discontinued	705.21
70.13	Panicum Field	19.61	-155.93	634.15	PALANI RANCH	NRFill, State	Discontinued	1173.06
70.14	Reservoir (5080)	19.63	-155.85	1548.78	PALANI RANCH	NRFill, State	Discontinued	768.94
70.16	Waiaha Stream*	19.63	-155.94	460.67	Hydronet	Hydronet, NRFill	Current	1225.28
70.3	Holualoa-Smith	19.61	-155.95	368.9	SMITH MRS TWIGG	NRFill, State	Discontinued	1081.58
70.4	Holualoa Camp	19.64	-155.88	1353.66	HUEHUE RANCH	NRFill, State	Discontinued	942.06
70.8	Rt Br Waiaha St	19.64	-155.91	1006.1	USGS	NRFill, State	Discontinued	1249.14
71	Honuaula	19.67	-155.88	1905.49	STATE DIV FTRY	Fill, NCDC, NRFill, State, State/NCDC	Current	753.74
73	Puu Lehua	19.57	-155.81	1478.66	GREENWELL ESTATE	Fill, NCDC, NRFill, State, State/NCDC	Discontinued	681.48
73.13	Honalo 1	19.55	-155.93	451.22	WODEHOUSE CN	NRFill, State	Discontinued	1462.11

73.26	Hokakano Beach	19.53	-155.96	0	ACKERMAN RANCH	NRFill, State	Discontinued	822.31
73.29	Kainaliu Upper*	19.53	-155.9	719.51	Hydronet	Hydronet, NRFill	Discontinued	1581.38
73.3	Mokuaikaua Rd	19.58	-155.92	603.66	BISHOP ESTATE	NRFill, State	Discontinued	1533.99
73.6	Honalo 2	19.55	-155.92	548.78	WODEHOUSE CN	NRFill, State	Discontinued	1544.28
73.7	Lehuula	19.54	-155.93	429.88	WALL RANCH	NRFill, State	Discontinued	1436.59
74	Kanahaha	19.59	-155.79	1542.68	GREENWELL ESTATE	Fill, NCDC, NRFill, State, State/NCDC	Discontinued	642.41
74.5	New Field	19.55	-155.81	1453.35	GREENWELL RANCH	NRFill, State	Discontinued	710.29
74.6	Kikiaeae	19.55	-155.78	1673.78	GREENWELL RANCH	NRFill, State	Discontinued	610.38
74.7	Momohaa (3875)	19.55	-155.86	1181.4	GREENWELL RANCH	NRFill, State	Discontinued	959.87
75	Ahua Umi	19.63	-155.78	1591.46	GREENWELL ESTATE	Fill, NCDC, NRFill, State, State/NCDC	Discontinued	621.1
75.1	Pta Kipuka Alala	19.67	-155.71	1641.77	RAWS	NRFill, RAWS	Current	464.24
76	Kulani Mauka	19.58	-155.45	2530.49	NWS	Fill, NCDC, State, State/NCDC	Current	869.81
77.8	Airport-K Ranch	19.52	-155.81	1432.93	KEALAKEKUA RANCH	NRFill, State	Discontinued	742.65
77.9	Orchard	19.52	-155.86	1143.29	GREENWELL RANCH	NRFill, State	Discontinued	1040.65
92.1	Huehue (1960)	19.75	-155.97	597.56	HUEHUE RANCH	Fill, NCDC, State, State/NCDC	Current	845.6
92.3	Halepiula 3	19.77	-155.9	713.41	PUUWAAWAA RANCH	NRFill, State	Discontinued	652.41
93.1	Puu Anahulu	19.82	-155.84	655.49	PUUWAAWAA RANCH	Fill, NCDC, State, State/NCDC	Discontinued	556.78

93.8	Kona Village	19.83	-155.99	12.2	KO VILLAGE RES	Fill, NCDC, State, State/NCDC	Current	275.11
94.1	Puu Waawaa	19.77	-155.84	838.41	PUUWAAWAA RANCH	Fill, NCDC, NRFill, State, State/NCDC	Discontinued	683.68
95.1	Puako	19.97	-155.85	1.52	GOTO ICHIRO	Fill, NCDC, NRFill, State/NCDC	Discontinued	224.84
95.8	Waikaloa	19.93	-155.79	295.73	BOISE CASCADE	Fill, NCDC, NRFill, State/NCDC	Current	333.98
97	Keamuku	19.84	-155.72	951.22	PARKER RANCH	Fill, NRFill, State	Discontinued	704.89
99	Pta West	19.77	-155.7	1307.93	RAWS	NRFill, RAWS	Current	561.19
100	Waikii*	19.86	-155.65	1417.38	PARKER RANCH	Fill, Hydronet, NRFill, State	Current	626.72
102.1	Puu Laau	19.83	-155.59	2268.29	STATE DIV FTRY	Fill, NCDC, State, State/NCDC	Discontinued	490.36